ORIGINAL PAPER

Altered White Matter Structure of the Dentatorubrothalamic Pathway in Children with Autistic Spectrum Disorders

**Jeong-Won Jeong · Diane C. Chugani ·
Michael E. Behen · Vijay N. Tiwari · Harry T. Chugani**

Abstract Neuropathological studies have demonstrated decreased Purkinje cells in cerebellar cortex and changes in the dentate nucleus of the cerebellum, the projection target for the Purkinje cells, in autistic spectrum disorders (ASD). The dentatorubrothalamic tract is formed by efferents from the dentate nucleus projecting toward the red nucleus with axon collaterals to this nucleus and continuing to innervate the ventral lateral and ventral anterior nuclei of the thalamus. In the current study, we assessed whether the dentatorubrothalamic tract is altered in ASD using Q-ball imaging (QBI). The QBI tractography was performed in 13 children with high functioning ASD (HFA), 11 children with low functioning ASD (LFA), and 14 typically developing children (TD). Regions of interest in dentate nucleus and red nucleus in both hemispheres were objectively placed to sort bilateral dorsal–rostral (DR), dorsal–caudal (DC), ventral–rostral (VR), and ventral–caudal (VC) portions of the dentatorubrothalamic pathway. Group differences in fractional anisotropy (FA), axial diffusivity, radial diffusivity, and fiber volume of individual pathways were analyzed. Significantly reduced FA was found in children with LFA and HFA, compared to the TD group in tracts originating in all four subdivisions of the right dentate nucleus. Tract-based morphometry (TBM) analysis demonstrated significant reductions of FA in caudal midbrain ($p < 0.0001$), dorsal–caudal dentate ($p = 0.0013$), and ventral–caudal dentate ($p = 0.0061$) on the right in the LFA group. The FA values in TBM segments of right VR and VC pathways were significantly correlated with communication skills in the combined HFA/LFA group, while there was a significant correlation found between TBM segments of right DR pathway and daily living skills ($r = 0.76$; $p = 0.004$). Decreased white matter integrity in dorsal portions of the dentatorubrothalamic tract may be related to motor features in ASD, while changes in the ventral portions are related more to communication behavior.

Keywords Dentatorubrothalamic tract · Dentate nucleus · Autism spectrum disorders · Q-ball imaging · Tract-based morphometry analysis

J.-W. Jeong · D. C. Chugani · M. E. Behen · V. N. Tiwari · H. T. Chugani
Carman and Ann Adams Department of Pediatrics, Wayne State University School of Medicine, Detroit, MI, USA

J.-W. Jeong · M. E. Behen · V. N. Tiwari · H. T. Chugani
Department of Neurology, Wayne State University School of Medicine, Detroit, MI, USA

D. C. Chugani · H. T. Chugani
Department of Radiology, Wayne State University School of Medicine, Detroit, MI, USA

J.-W. Jeong · D. C. Chugani · M. E. Behen · V. N. Tiwari · H. T. Chugani
Translational Imaging Laboratory, Children's Hospital of Michigan, Detroit, MI, USA

J.-W. Jeong (✉)
Departments of Pediatrics and Neurology, Wayne State University, PET Center, Children's Hospital of Michigan, 3901 Beaubien Blvd, Detroit, MI 48201, USA
e-mail: jeongwon@pet.wayne.edu

Introduction

Autism spectrum disorders (ASDs) are neurodevelopmental disorders characterized by impaired language development,

repetitive or stereotyped behaviors, and difficulties in socio-emotional interactions. There is a large body of evidence to support a role of the cerebellum in ASD based on neuropathology studies. Neuropathological studies have demonstrated reductions in Purkinje cells in the posterolateral cerebellar hemisphere in specimens from subjects with ASD [1–5]. Furthermore, Purkinje cell size has been reported to be decreased in autism brain specimens [6]. The dentate nuclei of the cerebellum lie in a key position of the cerebellum, serving to integrate inputs from the brainstem and spinal cord with Punkinje cell efferents [7].

Although previous neuropathological studies have clearly demonstrated alterations in Purkinje cells in ASD, the dentate nuclei did not show changes in cell number or size [4, 8]. However, both Purkinje cells and interneurons in the dentate nucleus show neurochemical changes, with lower expression of the GABA synthetic enzyme GAD67 in Purkinje cells and lower expression of GAD65 in the dentate nucleus [8, 9]. Thus, decreased GABA synthesis in both the Purkinje cells and dentate interneurons might be expected to result in decreased inhibitory input to the glutamatergic projection cells of the dentate that form the dentatorubrothalamic pathway. In addition, many structural and functional MRI studies have reported that children with ASD had significant morphological and functional variations in the cerebellum [10–17]. These studies have focused on changes in cortical regions of cerebellum without addressing the dentate nucleus, a region that plays a role in multiple functional domains such as motor function and cognition. Based upon anatomical tracing studies in nonhuman primates, Dum and Strick [18] demonstrated that dorsal portions of the dentate project to primary motor and premotor cortex, while caudal and ventral portions of the dentate nucleus project to prefrontal and parietal regions. A recent functional MRI (fMRI) study confirmed that a similar organization of the dentate nucleus is present in humans [19]. In that study, a motor task selectively activated the dorso-rostral dentate nucleus, whereas cognitive tasks produced predominant activation in the caudal region of the nucleus.

Diffusion tensor imaging (DTI) has been extensively utilized to quantitatively assess integrity of white matter (WM) in children with ASD. Many DTI studies have reported changes in fractional anisotropy (FA), mean diffusivity, axial diffusivity (AD), and radial diffusivity (RD) in ASD subjects compared to controls [20–26]. These changes were prominent in multiple major WM tracts including corpus callosum, arcuate fasciculus, uncinate fasciculus, internal capsule, external capsule, forceps minor, and corticospinal tract. However, all these studies were based on quantitative analysis of DTI measures in neuronal pathways that DTI can successfully image by tracking *single* fiber direction per voxel [27–29]. An example of a neuronal pathway that the conventional DTI technique fails to image

is the dentaterubro component of dentatorubrothalamic pathway which is a pathway of interest in this study, connecting the dentate nucleus of the cerebellum to the contralateral thalamus while sending collaterals to the contralateral red nucleus. Since left and right dentatorubrothalamic tracts cross in the midbrain, DTI has been inherently inadequate for resolving the neural architecture of this pathway. To date, this limitation has presented a significant obstacle for efforts to investigate this pathway using DTI technology.

Recent efforts to resolve diffusion imaging of complex crossing fiber–pathways have included the Q-ball imaging (QBI) technique in high angular resolution diffusion imaging (HARDI) acquisition. Several studies have shown that QBI isolates multiple crossing fibers of optic radiation, middle temporal gyrus, midbrain, prefrontal cortex, cingulum, semiovale, superior longitudinal fasciculus, pyramidal tract, and transverse pontocerbellar fibers in adults [30–35]. The QBI technique is model-independent and a considerably time-efficient method that can measure three-dimensional diffusion functions within each voxel by selectively sampling the diffusion signal on the spherical shell in q-space. The diffusion function denotes the probability of water molecule diffusion displacement at the voxel and has Fourier relationship with the measured diffusion signals in q-space. The QBI directly reconstructs a multimodal orientation distribution function (ODF) by projecting the diffusion function over radial dimensions. Local peaks of the reconstructed ODF are then used to indicate the directions of multiple fibers existing at the voxel [30, 31].

The present study utilized QBI to delineate the dentatorubrothalamic tract in children with high functioning autism (HFA), low functioning autism (LFA), and typically developing children (TD). To assess alterations of axonal integrity in motor and language/cognitive portions of the dentatorubrothalamic pathways, we subdivided the cerebellar dentate nucleus into four regions of interest (ROIs), dorso-rostral dentate (DRDN), dorso-caudal dentate (DCDN), ventro-rostral dentate (VRDN), and ventro-caudal dentate (VCDN). These four ROIs were originally defined in standard space that defines average locations for motor and non-motor domains in human dentate nucleus [19]. We objectively located these ROIs into individual subject space by applying a cerebellar-only normalization procedure using a spatially unbiased atlas template (SUIT) [36]. This normalization procedure was reported to provide 94% of maximum overlap of dentate nucleus across the participants [37]. The normalized ROIs were then utilized to seed different portions of the dentatorubrothalamic pathway. Alterations of individual pathways in axonal diffusivity such as FA, AD, RD, and fiber volume were studied along the entire course of the fiber and also in 1-mm segments by using a new method called tract-based morphometry (TBM) analysis [38, 39].

The TBM analysis was originally proposed to investigate subtle alterations in diffusion parameters of bilateral AF and cingulum [38]. This method spatially normalizes the fibers of multiple subjects in standard space and then registers the coordinates of individual fibers to those of a group standard fiber, followed by statistical analysis of DTI measures only at the common coordinates of group subjects. Unlike other voxel-based analysis such as tract-based spatial statistics [40], this analysis uses white matter trajectory for between-subject registration. Use of fiber trajectories to register the values of DTI parameters across the subjects may yield less registration errors, which highly depend on the differences of individual morphology and be more suitable for performing multiple comparisons for group analyses since the parameter values are directly sampled at anatomically equivalent regions. In the current study, we hypothesized that segmentwise approach like the TBM analysis might be useful to detect subtle changes in axonal anisotropy existing in the dentatorubrothalamic pathways. We further hypothesized that reductions in the dorsal–ventral portions of LFA and HFA groups underlying reduced integrity in dorsal portion may be related to motor features, while changes in the ventral portion are related more to communication behavior.

Methods and Materials

Subjects

Thirteen children with a diagnosis of HFA (age, 5.2± 3.4 years; range, 1.9–13.3 years, 11 boys), 11 children with a diagnosis of LFA (age, 4.1±2.1; range 2.1–8.5 years, 10 boys), and 14 typically developing children (TD group, age 6.8±3.1, range=4.3–13.2 years, 11 boys) were studied. All children with ASD were referred from the Children's Hospital of Michigan Neurology Clinic. Inclusion criteria for the study required that children with ASD meet or exceed the clinical cutoff on sections (a) Qualitative Abnormalities in Reciprocal Social Behavior and (b) Restricted, Repetitive, and Stereotyped Patterns of Behavior of the Autism Diagnostic Interview Revised (ADI-R). All but three of the children (all three in the HFA group, see below) also met or exceeded the clinical cutoff for (c) Qualitative Abnormalities in Communication. Neurological disorders were excluded in the ASD groups, including seizure disorders (abnormal EEGs without seizures were not excluded), PKU, tuberous sclerosis complex, Rett syndrome, Fragile X, Down syndrome, and traumatic brain injury. Children meeting the criteria for ASD were divided into LFA and HFA groups defined by level of intellect and adaptive behavior. For the HFA group, children had to score above the borderline and at least at the low average range (>79) on

Full Scale Intelligence Quotient (FSIQ) and have a Vineland Adaptive Behavior Composite (ABC) greater than 69 (above the impaired range). The reason that adaptive behavior for the HFA group had a threshold of >69 is that measures of adaptive behavior are often reduced relative to FSIQ in individuals with autism (particularly in HFA). For FSIQ, we selected the threshold of FSIQ >79 in order to ensure that the children in the HFA group were clearly high functioning (i.e., above borderline range). For the LFA group, all had scores that placed them in the cognitively impaired (FSIQ <70) range and adaptive behavior scores which placed them in the impaired range (ABC <70). The descriptive and inferential statistics for neurobehavioral characteristics obtained from children with HFA and LFA are summarized in Table 1.

Inclusion criteria for the TD group included the following: (1) measured intellectual functioning within normal limits, FSIQ ≥85; (2) normal neurological screening; and (3) absence of any current or historical medical or psychiatric diagnoses. TD children were obtained through active recruitment. Children with any of the following were excluded from the study: (1) history of seizures; (2) focal deficits on clinical examination by a pediatric neurologist; (3) MRI interpretated as abnormal by a pediatric neuroradiologist; (4) dysmorphic features suggestive of a genetic syndrome; (5) history of prematurity or perinatal hypoxic–ischemic event; and (6) an inborn error of metabolism.

All children in the study were right-handed. The groups did not differ on age (p=0.45). Because the scans of children with ASD were clinical MRI studies, sedation was used as necessary by the sedation team at Children's Hospital of Michigan. None of the TD children were sedated for the MRI. Younger TD children were scanned while sleeping, and all TD children were monitored for movement during scan. If there was significant movement, either the MRI was repeated or the subject was excluded from the study. Written and informed consent was obtained from one of the parents or legal guardians of the TD participants. The Human Investigation Committee at Wayne State University granted permission for the retrieval and analysis of the clinical data and MRI scans of children with ASD.

Diagnostic/Developmental Assessments

The ADI-R [41] is a clinical semi-structured diagnostic instrument for assessing autism spectrum problems in children and adults, focusing on behavior in three main areas: qualities of reciprocal social interaction; communication and language; and restricted and repetitive, stereotyped interests and behaviors. Psychometric properties of the measure support the use of the ADI-R for children and adults with mental ages from about 18 months and above. The ADI-R

Table 1 Neurobehavioral characteristics between HFA and LFA groups

Domain	Subdomain	HFA	LFA	p value
Global intellectual	FSIQ	103.6 (7.8)	54.6 (4.9)	0.000
Adaptive behavior (VABS-2)	Communication	78.1 (11.2)	57.1 (6.1)	0.000
	Daily living skills	86.8 (8.9)	70.0 (9.9)	0.000
	Socialization	78.7 (10.6)	62.7 (5.2)	0.000
	Motor skills	81.1 (11.9)	69.5 (10.9)	0.037
	Overall adaptive behavior composite (ABC)	78.1 (7.1)	62.0 (3.2)	0.000
Magnitude of autistic symptoms (SRS)	Social awareness	61.4 (12.4)	68.7 (7.9)	0.594
	Social cognition	71.1 (8.0)	71.8 (7.1)	0.976
	Social communication	78 (9.1)	76.1 (6.2)	0.862
	Social motivation	71.1 (11.1)	74.1 (3.0)	0.790
	Autistic mannerisms	73.5 (8.1)	76.8 (5.1)	0.866
	Total score	72.8 (7.7)	75.2 (4.0)	0.788

was used in this study to confirm a diagnosis of ASD in all patients studied (see above).

Social Responsiveness Scale (SRS) [42, 43] is a 65-item caregiver rating scale that measures the severity of autism spectrum symptoms as they occur in natural social settings. The measure has been demonstrated to have good psychometric properties [42, 43]. The subscales and the total scale score are used in the present study to describe the severity of symptoms across the two groups of children with ASDs. For measurement of global intellectual function, children initially received the Wechsler Intelligence Scales for Children—Fourth Edition (WISC-IV) or Wechsler Pre-primary and Pre-school Intelligence Scales—Third Edition (WPPSI-III), depending upon age. Children unable to reliably complete the Wechsler protocol were administered the Mullen Scales of Early Learning.

The WPPSI-III is an individually administered clinical instrument for assessing the intellectual functioning of pre-primary and pre-school-aged children, aged 2.11 to 7.3 years. The psychometric properties of the WPPSI-III are well-established [44]. The WPPSI-III was used in this study as a measure of global intellectual functioning in children 36 through 71 months of age.

The WISC-IV [45] is an individually administered clinical instrument for assessing the intellectual functioning of children and adolescents aged 6.0–16.11 years. The psychometric properties of the WISC-III are well-established [46], and the measure is widely used in both clinical and research populations. The WISC-IV was used in this study as a measure of global intellectual functioning in children over 71 months of age.

The Mullen Scales of Early Learning (MSEL) is a developmentally integrated system that assesses language, motor, and perceptual abilities from birth to 68 months. The measure has five scales, which provide information for the following domains: gross motor, visual reception, fine

motor, expressive language, and receptive language as well as an overall measure of general cognitive ability which is derived from the cognitive scales. Psychometric data for the measure are good, and the measure is widely used in both research and clinical settings with pervasive developmental disorder samples [47]. The MSEL was used in this study to assess the global cognitive functioning in children in whom reliable assessment with the Wechsler series was not possible.

The Vineland Adaptive Behavior Scales (VABS) [48] is a semi-structured interview administered to the primary caregiver regarding communication, daily living skills, socialization, and motor skills. An overall adaptive behavior composite is also provided. The measure is widely used in clinical and research samples, and the psychometric properties are well-established. The measure is particularly useful in the assessment of children with pervasive developmental problems in whom standardized measures are not always reliable [49]. The VABS was used to quantify adaptive behavior functioning across all four domains, as well as overall adaptive behavior functioning for group definition and for examining associations between DTI metrics and developmental dimensions.

MRI Data Acquisition

Whole brain HARDI acquisition was acquired using a 3-T Signa EXCITE scanner (GE Healthcare, Waukesha, WI) equipped with an eight-channel phased-array head coil. A multislice single-shot echo-planer spin-echo sequence was employed to obtain measurements at a diffusion weighting of $b=1,000$ s/mm^2 and 55 diffusion gradient directions, TR/TE=12,500/88.7 ms, and voxel size=1.88×1.88×3 mm. An additional acquisition at $b=0$ s/mm^2 was also obtained. Parallel imaging of DW data acquired with the eight-channel EXCITE head coil was accomplished using the

array spatial sensitivity encoding technique with an acceleration factor of 2. Total imaging time was about 11 min. For anatomical reference, a three-dimensional fast spoiled gradient echo sequence (FSPGR) was acquired for each subject at TR/TE/TI of 9.12/3.66/400 ms, slice thickness of 1.2 mm, and planar resolution of 0.94×0.94 mm^2.

Q-Ball Reconstruction and Tractography

The present study produced the q-ball ODF maps using regularized and fast analytical algorithm [50]. The diffusion ODF for each voxel was reconstructed by the spherical harmonic approach with a regularization based on the Laplace–Beltrami operator. The spherical harmonic order for the ODF decomposition was set to be 8 [50]. The regularization parameter was optimized at 0.001 in order to achieve the highest sensitivity to resolve multiple fibers in the QBI data. The obtained ODF had 363 directions generated from six-fold tessellated icosahedrons, offering an angular resolution of approximately 9°. The generalized fractional anisotropy (gFA) and the peak diffusion direction of the ODF were computed to evaluate the geometric properties of the ODF of each voxel [30]. The gFA was calculated by the standard deviation of the ODF divided by the root mean square of the ODF, which quantifies the degree of anisotropy in the ODF. Three maximum local peaks of the ODF were determined to resolve major fiber directions existing at the voxel and were utilized for subsequent tractography.

The tractography of QBI was performed by a modified streamline tracking algorithm [28], which was implemented on the software package of DSI studio (http://dsi-studio.labsolver.org). At each seeding point, tracking was started in the direction of the most prominent fiber. The step size was 0.2 voxel width, turn angle threshold was 60°, and the seeding number was 50,000. The propagation direction was calculated by applying trilinear interpolation on the fiber orientations provided from eight nearby voxels of the current point. For each nearby voxel, only the fiber orientation that had the smallest turning angle was considered for interpolation. Voxels with gFA less than 0.02 were excluded for interpolation. In order to smooth the tracts, each subsequent direction was determined by the previous direction with 0.5 weighting and incoming direction with 0.5 weighting. To eliminate possible false fibers, the fibers were filtered by their relative ratio provided by the ODF decomposition method [51].

Figure 1 illustrates the objective procedure to locate the standardized ROIs of bilateral dentate nuclei (seeding ROI) and red nuclei (sorting ROI) across subjects. Four subdivisions of the dentate nucleus in template space (DRDN, DCDN, VRDN, and VCDN) [19] were separately transformed into the FSPGR space of individual subjects by applying the inverse of deformation field that fit the

cerebellar cortex of the individual FSPGR image to that of the SUIT space [36] while ensuring a near-perfect overlap between the dentate nucleus of the FSPGR image and a dentate template that was developed as an average of the 23 healthy controls [37]. The border between the rostral and caudal dentate was set between $y=-58$ and $y=-59$, which corresponds to the middle of the maximum extension of the dentate atlas space in the rostro-caudal extension in the axial plane ($y=-48$ to -68 mm). The border between the ventral and dorsal dentate was set between $z=-35$ and $z=-36$ which corresponds to the middle of the maximum extension of the dentate atlas space in the ventro-dorsal extension ($z=-30$ to -41 mm) in the sagittal plane. The resulting volumes of DRDN, DCDN, VRDN, and VCDN ROI are 351, 403, 293, and 314 mm^3, respectively. This spatial normalization using the SUIT space template showed 94%, 79%, and 29.7% of maximal overlap across participants for dentate nucleus, interposed nucleus, and fastigial nucleus where the average volume of each nucleus was 1,380, 160, and 13 mm^3. The spatial normalization of relatively small structure like fastigial nucleus became limited in the framework of SUIT template space. However, the spatial normalization of large deep nuclei like dentate was successful to achieve that the center of mass of dentate nucleus varied with a standard deviation of ~1.5 mm in each spatial direction (e.g., average $x/y/z$ size of dentate 13/19.3/14.3 mm [37]).

The SUIT normalized ROIs in the FSPGR space were then moved to the b0 space by applying the affine transformation obtained between the FSPGR and b0 images. The seeding points were uniformly distributed within each of four dentate ROIs located in the b0 space (density=1/mm^3). An ROI filtering approach was utilized to sort the tracts connecting each of the dentate ROIs to the contralateral red nucleus. Montreal Neurological Institute (MNI) space ROIs delineating the red nucleus (WFU PickAtlas, www.fmri.wfubmc.edu/cms/software) were objectively placed in the subject's native space by applying inverse of spatial deformation obtained between the subject's b0 image and MNI b0 template. The fibers for each dentatorubrothalamic tract were sorted to include fibers passing the dentate nucleus and the contralateral red nucleus ROIs.

Whole Pathway Analysis

The average FA, AD, RD, and fiber volume of individual dentatorubrothalamic pathways were measured across subjects and tested using two-sample t test. To investigate the asymmetry of measure across hemispheres, statistical significance of the degree of the lateralization (i.e., $2 \times$ (left−right)/(left+right)) was examined for each pathway. Analysis of the difference in individual measures between the left and right hemispheres of each pathway and the groups was performed using repeated measure ANOVA. The subject
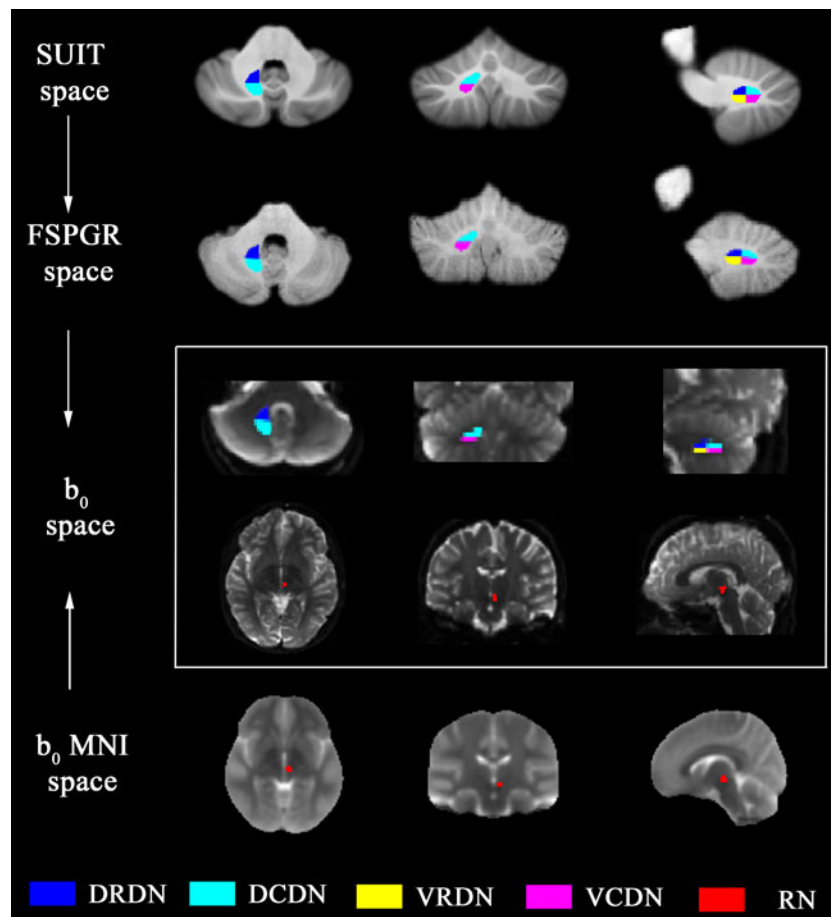
Fig. 1 Procedure for localizing standardized ROIs in dentate nuclei and red nuclei across subjects. *White box* indicates the b0 image of individual subject's head space in which whole brain QBI tractography was performed. ROIs of four dentate segments defined in SUIT space [*blue*: dorso-rostral (DC), *cyan*: dorso-caudal (DC), *yellow*: ventro-rostral (VR), *magenta*: ventro-caudal (VC)] were initially transformed into FSPGR space for an individual subject's head space by applying the inverse of deformation field that was obtained from the T1 template image of SUIT space to the FSPGR image. The resulting ROIs were then transformed to the b0 space by applying the affine transformation between FSPGR and b0 images. The ROIs located in the b0 space were finally used to seed separate four divisions of the dentatorubrothalamic tract in each hemisphere. The ROIs for red nuclei in b0 MNI space (*red*) were transformed into the b0 space by applying the inverse of deformation field that was obtained from the b0 MNI template to the b0 image of individual subject. The ROIs were then utilized to sort the subdivisions of the dentatorubrothalamic tract that originated from the ROIs of contralateral dentate nuclei

average of each pathway was set as a within-subjects factor (4 pathways×2 sides) and the group as a between-subjects factor. Only results that survived Bonferroni correction are presented. SPSS 18.0 was used for all statistical analyses.

Tract-Based Morphometry Analysis

To investigate focal alterations of the diffusivity parameter in the course of individual pathways, we employed the TBM analysis that is a coordinate-wise statistical analysis to compare DTI parameters of multiple subjects at a common coordinate system of specific fiber bundles [38, 39]. Initially, the fibers of a given pathway were spatially normalized from the b0 space to the SUIT space by applying the deformation field that was used for the ROI placement. Next, the most representative fiber from the normalized

pathway was selected as the "prototype fiber". Uniformly sampled points on the prototype define the common coordinates, "*s*". Independent statistical tests were performed at these common coordinates.

In the present study, the average length fiber penetrating the highest fiber density region of a given fiber bundle in the TD group was selected as a "prototype" for that particular bundle and was used to define the common arc length coordinates for that bundle. Common coordinates were placed every 1 mm arc length of the prototype fiber since single voxel size in SUIT space was set to 1 mm. These coordinates were used as "reference points" to register the corresponding coordinates of individual fibers of the respective tracts in each subject by using the Hungarian matching algorithm [38]. Subsequently, the DTI parameters (FA, AD, and RD) of each fiber tract at each coordinate were evaluated in each subject, and group

differences were examined by two-sample t test. Bonferroni–Hom adjustment at $\alpha=0.05$ was applied to correct the p value for multiple comparions, p_c [52].

Comparison of DTI Parameters with Behavior Parameters

Pearson partial correlations (controlling for age) were used to test for relationships between FA for the DRDN, DCDN, VRDN, and VCDN and global IQ and adaptive behavior domains (communication, daily living, socialization, and motor skills). Since the groups did not differ on severity of autistic symptoms, and to reduce the number of comparisons, correlations with the SRS subdomains were not conducted. Separate correlations were run for the HFA and LFA groups and were run within the combined HFA–LFA group as well. In order to control for multiple comparisons, only those correlations significant at $p<0.01$ are reported.

Results

The QBI was able to isolate two orientation components crossing in the caudal midbrain and sort fiber bundles connecting each of the dentate subregions to the contralateral red nuclei in all subjects. Figure 2 shows an example of a

QBI-reconstructed fiber direction map and ODF along with bilateral dentatorubrothalamic pathways that were obtained by the above-described ROI placement method. The ANOVA analysis showed a significant interaction between group and FA ($F=2.646$, $p=0.007$), volume ($F=2.442$, $p=0.013$), and RD ($F=2.231$, $p=0.023$) but no interaction for the AD. Post hoc analysis revealed a statistically significant group difference in FA ($p<0.001$ and 0.001 for TD vs. HFA and TD vs. LFA, respectively) and in RD ($p=0.007$ for TD vs. HFA). No significant group difference in the asymmetry of DTI indices (FA, volume, AD, and RD) was found for any of the four pathways.

Group comparisons for FA, AD, RD, and fiber volume of the fiber pathways are summarized in Table 2. There was a significant reduction in FA of all four subdivisions of the right fiber pathways in both HFA and LFA groups. There was also decreased FA in the left DRDN pathway for both HFA and LFA groups and in left DCDN pathway for LFA group. RD was increased in the right DRDN pathway and in left and right DCDN pathways in both ASD groups. RD was also increased in left VRDN and VCDN pathways in the HFA group, whereas RD was increased in right VCDN pathway in the LFA group. These findings were supported by subsequent TBM analyses presented in Figs. 3, 4, and 5. For instance, the FA reductions of both HFA and LFA

Fig. 2 QBI tractography for the dentatorubrothalamic pathway. a Fiber orientation map reconstructed by the QBI. Yellow box indicates the voxels that the dentatorubrothalamic pathway penetrates near caudal midbrain. The ODFs show two crossing fibers at those voxels. The ODFs were attached to demonstrate the reliability of isolated crossing fiber components. b Representative example of bilateral dentatorubrothalamic pathways obtained from a typically developing child (8.2-year-old male). The ROIs of Fig. 1 were used to sort corresponding pathways
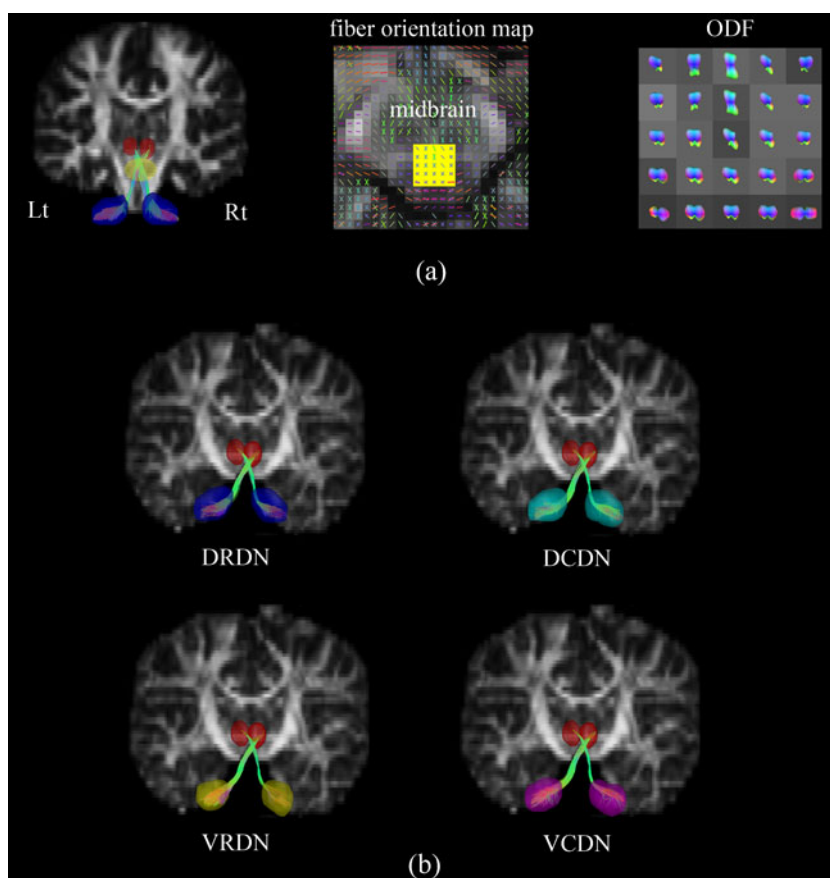
Table 2 FA, AD, RD, and volume of fiber pathways for all groups and their statistical significance in two-sample *t* test

DN	Side	Group	FA		AD		RD		VOL	
			Mean, SD	*t* score, *p* value	Mean, SD	*t* score, *p* value	Mean, SD	*t* score, *p* value	Mean, SD	*t* score, *p* value
DR	Lt	TD	0.428, 0.038		1.428, 0.169		0.772, 0.162		1,688; 580	
		HFA	0.377, 0.068	2.37, 0.027	1.518, 0.278	−0.99, 0.332	0.938, 0.278	−1.87, 0.074	1,962; 986	−0.87, 0.394
		LFA	0.382, 0.070	2.13, 0.043	1.428, 0.262	0.00, 0.997	0.848, 0.266	−0.90, 0.375	3,025; 3,568	−1.38, 0.178
	Rt	TD	0.508, 0.039		1.264, 0.066		0.552, 0.058		2,591; 2,055	
		HFA	0.443, 0.041	**3.98, 0.001***	1.292, 0.111	−0.79, 0.440	0.656, 0.090	**−3.52, 0.002***	2,152; 892	0.66, 0.516
		LFA	0.431, 0.056	**4.11, 0.000***	1.238, 0.066	1.03, 0.315	0.630, 0.084	**−2.83, 0.009***	2,436; 981	0.25, 0.808
DC	Lt	TD	0.400, 0.042		1.467, 0.187		0.837, 0.175		1,861; 674	
		HFA	0.343, 0.068	1.62, 0.120	1.604, 0.260	−1.53, 0.139	1.048, 0.261	**−2.42, 0.024**	1,827; 1,106	0.10, 0.924
		LFA	0.314, 0.077	**2.36, 0.026**	1.546, 0.234	−0.97, 0.339	1.015, 0.227	**−2.29, 0.031**	1,763; 824	0.34, 0.738
	Rt	TD	0.455, 0.072		1.233, 0.212		0.581, 0.131		2,891; 2,300	
		HFA	0.416, 0.038	**3.59, 0.003***	1.333, 0.166	−1.29, 0.211	0.705, 0.130	**−2.36, 0.027**	2,173; 1,140	0.95, 0.354
		LFA	0.396, 0.055	**3.66, 0.001***	1.252, 0.126	−0.29, 0.778	0.676, 0.092	**−2.16, 0.041**	2,288; 716	0.90, 0.375
VR	Lt	TD	0.423, 0.042		1.385, 0.180		0.748, 0.164		1,614; 645	
		HFA	0.371, 0.063	1.90, 0.070	1.478, 0.220	−1.16, 0.259	0.917, 0.228	**−2.16, 0.042**	1,953; 942	−1.07, 0.297
		LFA	0.374, 0.076	2.06, 0.050	1.444, 0.250	−0.70, 0.489	0.875, 0.264	−1.51, 0.145	1,836; 765	−0.82, 0.422
	Rt	TD	0.485, 0.061		1.248, 0.091		0.572, 0.078		2,499; 1,992	
		HFA	0.445, 0.037	**2.49, 0.020**	1.212, 0.058	1.13, 0.271	0.609, 0.065	−1.27, 0.218	2,507; 1,061	−0.01, 0.992
		LFA	0.428, 0.046	**2.73, 0.011**	1.219, 0.052	1.01, 0.322	0.625, 0.065	−1.94, 0.064	2,463; 556	0.06, 0.950
VC	Lt	TD	0.404, 0.042		1.418, 0.159		0.796, 0.150		2,170; 992	
		HFA	0.349, 0.067	1.41, 0.171	1.526, 0.245	−1.33, 0.197	0.979, 0.254	**−2.25, 0.034**	2,416; 1,091	−0.59, 0.562
		LFA	0.351, 0.070	1.86, 0.074	1.482, 0.230	−0.85, 0.402	0.935, 0.251	−1.76, 0.090	2,047; 973	0.33, 0.746
	Rt	TD	0.454, 0.077		1.221, 0.210		0.575, 0.133		3,134; 2,406	
		HFA	0.418, 0.034	**2.48, 0.021**	1.291, 0.129	−0.96, 0.345	0.678, 0.111	−2.07, 0.050	2,590; 1,165	0.69, 0.499
		LFA	0.405, 0.055	**2.37, 0.026**	1.257, 0.075	−0.58, 0.564	0.672, 0.080	**−2.27, 0.032**	2,862; 714	0.39, 0.699

The *t* score and *p* value compared to TD group are given in bold face whenever the corresponding *p* value<0.05 (two-tailed, α=0.05). Negative sign indicates an increase in ASDs compared to TD

DN dentate, *DR* dorso-rostral, *DC* dorso-caudal, *VR* ventro-rostral, *VC* ventro-caudal, *Lt* left, *Rt* right, *TD* typical development, *HFA* high functioning autism, *LFA* low functioning autism, *FA* fractional anisotropy, *AD* axial diffusivity (10^{-3} mm/s^2), *RD* radial diffusivity (10^{-3} mm/s^2), *VOL* volume (mm^3).

*p values<0.005

groups compared to the TD group were apparently restricted in two clusters of focal coordinates in the right DRDN pathway, dorsal–caudal dentate ($6 \leq s \leq 18$ mm peaked at $s=9$ mm), and caudal midbrain ($38 \leq s \leq 54$ peaked $s=40$ mm) as demarked by square brackets in Fig. 3a. Both HFA and LFA groups showed similar reductions in the caudal dentate ($p=0.006$, $p_c=0.029$ as shown in Fig. 3b). Interestingly, the LFA group showed a more significant reduction in the caudal midbrain ($p<0.0001$, $p_c=0.0013$ as shown in the right column of Fig. 3b). The TBM analyses for right DCDN and VCDN (Figs. 4 and 5) found that compared to the TD group, both HFA and LFA groups showed significant reductions of FA in the cluster of focal coordinates in the right dorsal–caudal dentate ($0 \leq s \leq 6$ mm peaked at $s=2$ mm of Fig. 4a) and the cluster of focal coordinates in right ventral caudal dentate ($0 \leq s \leq 8$ mm peaked at $s=0$ mm of

Fig. 5a) where brackets in Figs. 4a and 5a indicate exact locations of cluster segments showing significant group differences. Furthermore, the LFA group showed the most significant FA reductions in right dorsal–caudal dentate ($p=0.0013$, $p_c=0.05$ as shown in the right column of Fig. 4b). The HFA group showed the most significant reductions in right ventro-caudal dentate ($p=0.006$, $p_c=0.029$ as shown in the left column of Fig. 5b).

Table 3 summarizes the correlation analysis between behavioral domains and FA values for segments identified by TBM in four pathways. In the combined HFA–LFA group, significant positive correlations were found between FA for the cluster of segments of the right VRDN ($r=0.60$, $p=0.002$) and right VCDN ($r=0.57$, $p=0.005$) and communication skills; trends approached significance for the cluster of segments of right VRDN and right VCDN and overall
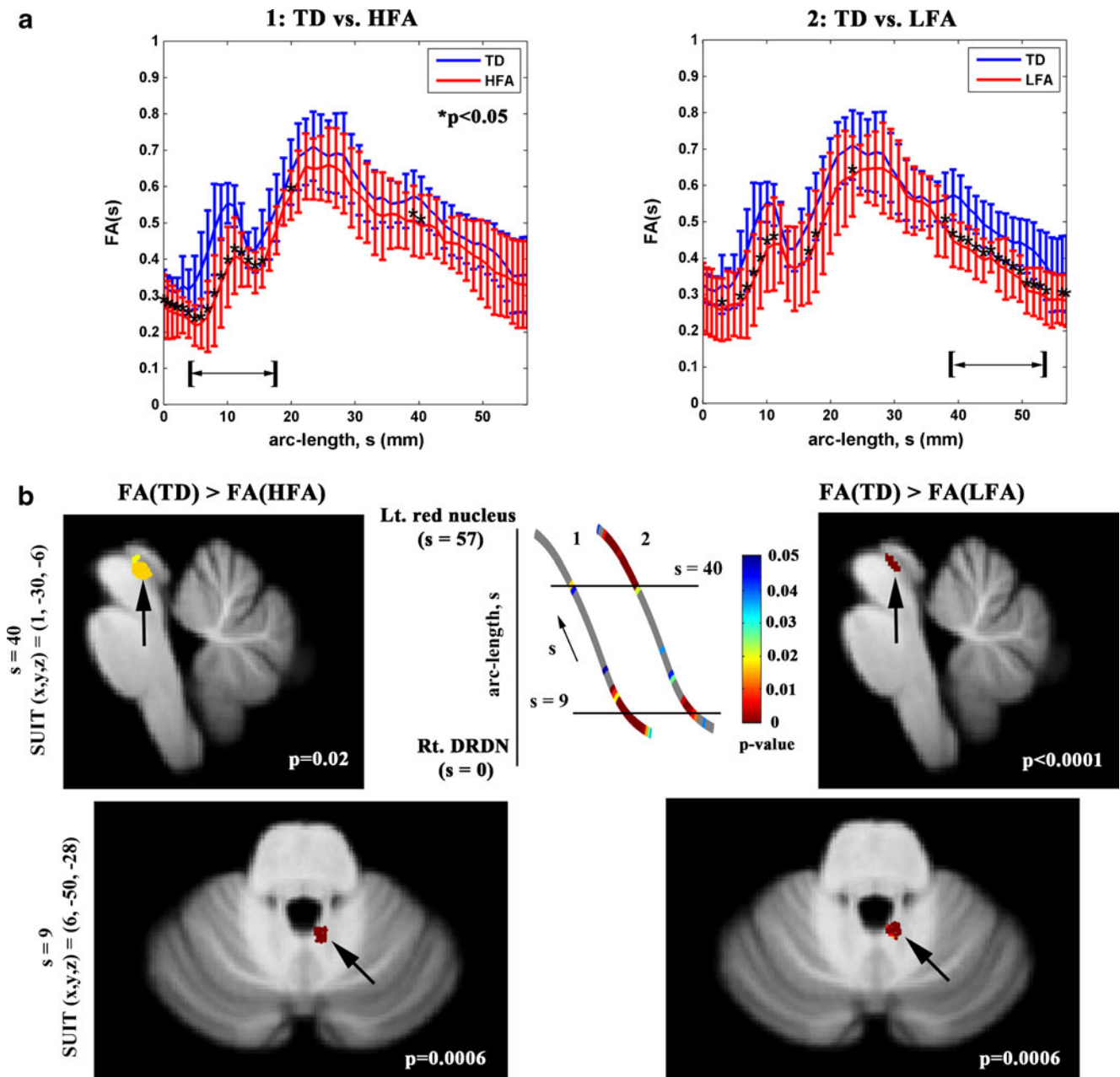
Fig. 3 Fiber tract fractional anisotropy (*FA*) estimates from TBM analysis for right dorso-rostral dentate (DRDN) pathway. **a** The group mean and standard deviation of FA at each common arc length coordinate are plotted at the respective common coordinates, (*left*) TD vs. HFA and (*right*) TD vs. LFA. *Block asteroids* and *brackets* indicate the coordinates and their clusters showing significant difference, *p*<0.05. **b** For the comparison of the TD group, FA is greater than in the HFA group (*1: left*) and the LFA group (*2: right*), the *p* value for the group

difference at each common arc length coordinate is overlaid on a prototype fiber. Note that we define the first common arc length coordinate (*s*=0 mm) at right DRDN. Two clusters of coordinates (peaked at *s*=9 and 40 mm) showed significant reduction in FA for HFA and LFA. Cross-sectional images show exact locations of two coordinates showing the highest significance (*s*=9 and 40 marked by *black arrows*) in SUIT space whose FA is significantly reduced in HFA (*left*) and LFT (*right*) compared to TD

adaptive behavior (*r*=0.46, *p*=0.02 and *r*=0.45, *p*=0.03, respectively). For the HFA group, while none of the correlations found for the combined group remained significant, the association between the right ventral segments and communication skills remained (*r*=0.62, *p*=0.043; *r*=0.54,

p=0.049). A trend between right DRDN and motor skills was also found (*r*=0.52, *p*=0.049). For the LFA group, there was a significant correlation found between the segments of right DRDN and daily living skills (*r*=0.76, *p*=0.004). The correlation coefficients between behavioral domains and RD
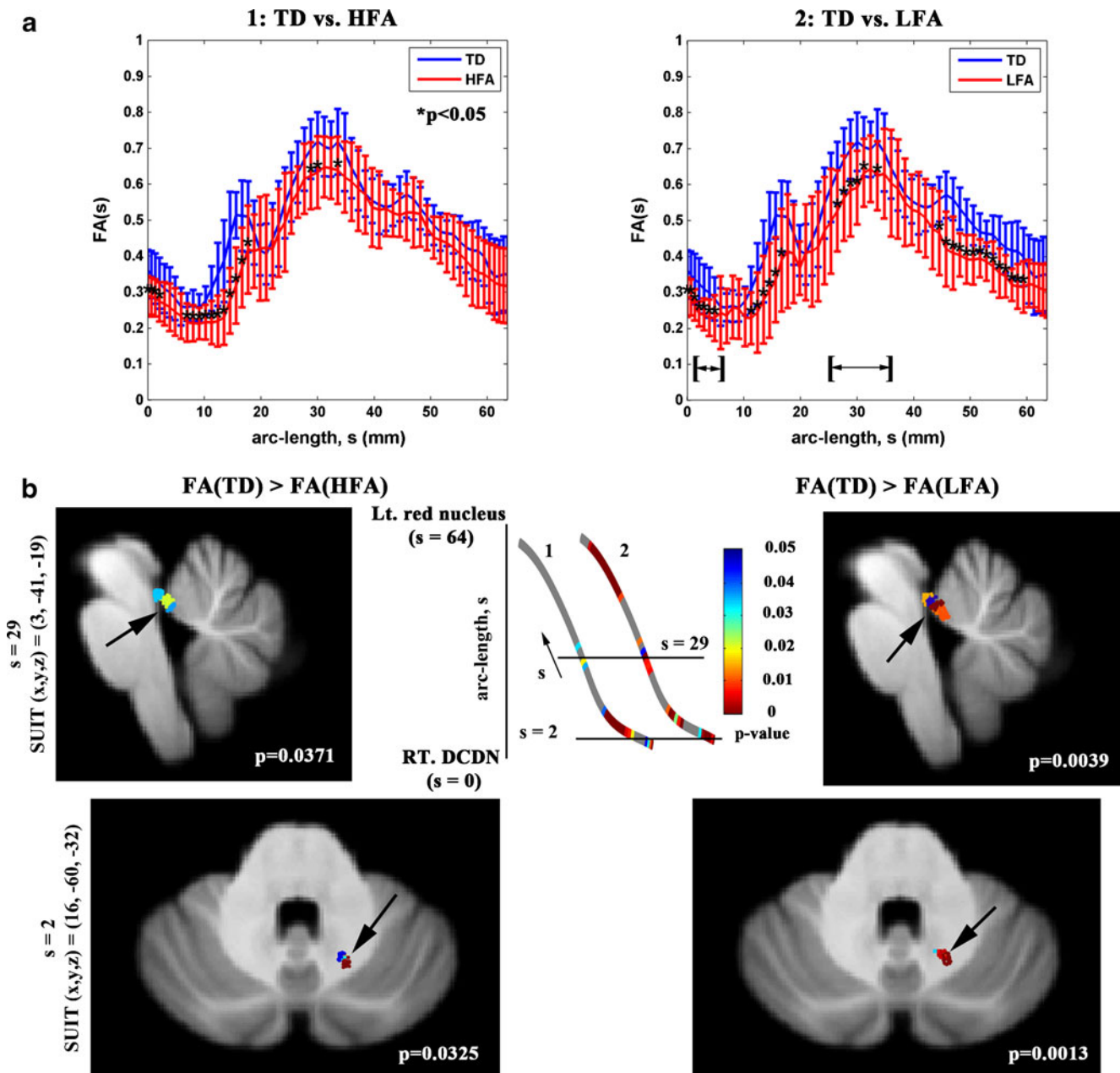
Fig. 4 Fiber tract fractional anisotropy (*FA*) estimates from TBM analysis for right dorso-caudal dentate (DCDN) pathway. **a** The group mean and standard deviation of FA at each common arc length coordinate are plotted at the respective common coordinates, (*left*) TD vs. HFA and (*right*) TD vs. LFA. *Block asteroids* and *brackets* indicate the coordinates and their clusters showing significant difference, *p*<0.05. **b** For the comparison of the TD group, FA is greater than in the HFA group (*1: left*) and the LFA group (*2: right*), the *p* value for the group

difference at each common arc length coordinate is overlaid on a prototype fiber. Note that we define the first common arc length coordinate (*s*=0 mm) at right DCDN. Two clusters of coordinates (peaked at *s*=2 and 29 mm) showed significant reduction in FA for HFA and LFA. Cross-sectional images show exact locations of two coordinates showing the highest significance (*s*=2 and 29 marked by *black arrows*) in SUIT space whose FA is significantly reduced in HFA (*left*) and LFT (*right*) compared to TD

values of the TBM segments are presented in Table 4. We found that (1) the RD value of right DRDN in LFA group was correlated with daily living skills at *p*=0.041 and (2) communication in HFA group was correlated with the RD of right VRDN at *p*=0.030. However, these correlations were less significant compared to those of FA.

Discussion

This study demonstrates the feasibility of the QBI technique to isolate dentatorubrothalamic tracts in children. Compared with the age–gender-matched TD group, the ASD groups showed significantly reduced white matter integrity in the
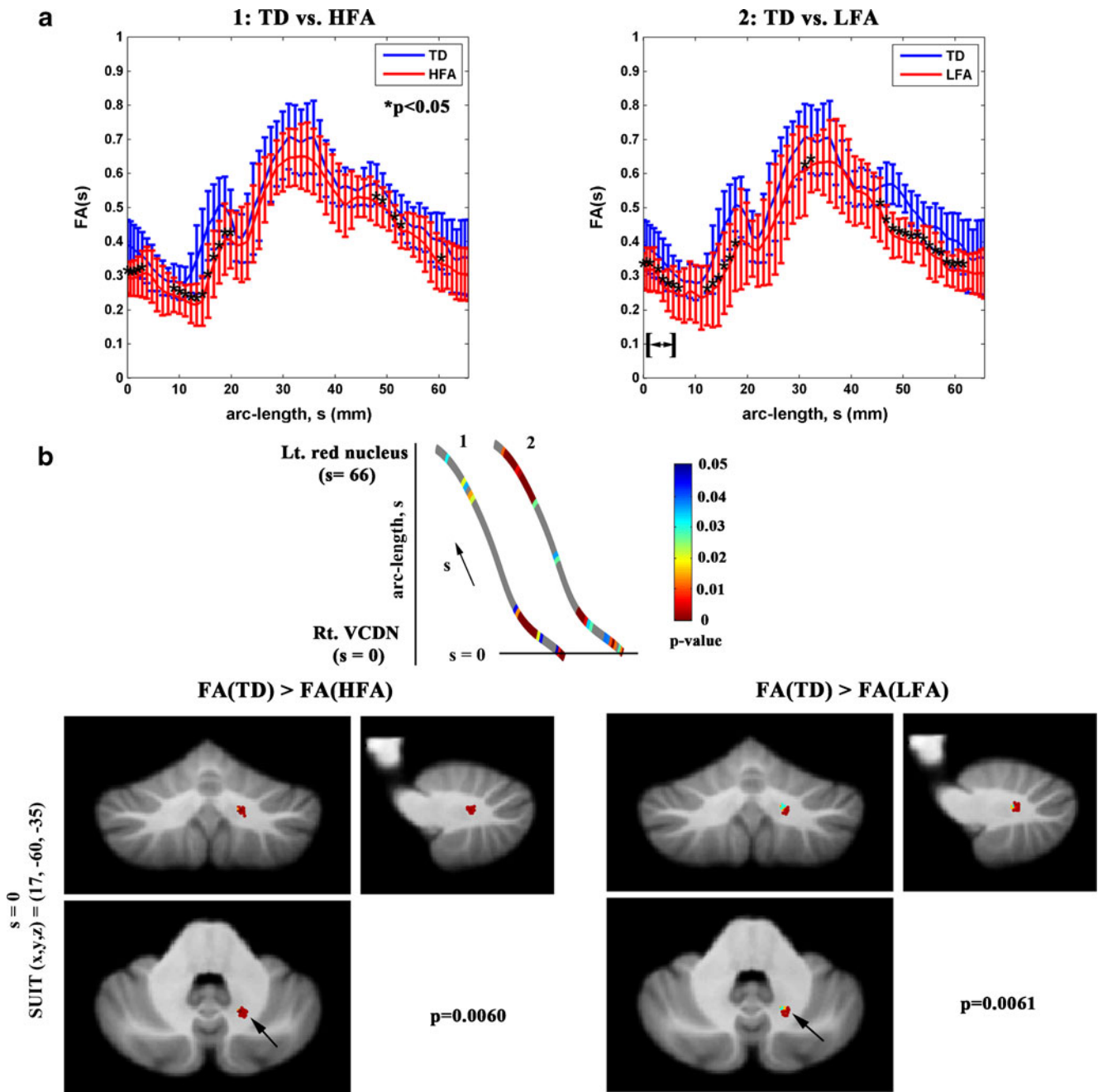
Fig. 5 Fiber tract fractional anisotropy (*FA*) estimates from TBM analysis for right ventro-caudal dentate (VCDN) pathway. **a** The group mean and standard deviation of FA at each common arc length coordinate are plotted at the respective common coordinates, (*left*) TD vs. HFA and (*right*) TD vs. LFA. *Block asteroids* and *brackets* indicate the coordinates and their clusters showing significant difference, *p*<0.05. **b** For the comparison of the TD group, FA is greater than in the HFA group (*1*: *left*) and the LFA group (*2*: *right*), the *p* value for the group difference at each common arc length coordinate is overlaid on a prototype fiber. Note that we define the first common arc length coordinate (*s*=0 mm) at right VCDN. 3-D cross-sectional images show exact locations of *s*=0 coordinate showing the highest significance (marked by *black arrows*) in SUIT space whose FA is significantly reduced in HFA (*left*) and LFT (*right*) compared to TD

right dorsal–rostral, dorsal–caudal, ventral–rostral, and ventral–caudal portions of the dentatorubrothalamic pathway. Subsequent TBM analysis confirmed the reductions in right dorsal midbrain, dorsal–caudal dentate, and ventral–caudal dentate. Decreased white matter integrity in dorsal portions of the dentatorubrothalamic tract may be related to motor features in ASDs, while changes in the ventral portions are related more to communication behavior.

Lower FA and higher RD at focal segments of dentatorubrothalamic tracts in ASD groups suggest decreased axon diameter and/or decreased myelinaton. Thinner axons disproportionately decrease the axon volume and increase

Table 3 Correlation between behavioral domains and FA values of TBM segments

Domain	Group	Rt. DRDN $0 \leq s \leq 10$ SUIT $(x, y, z) = (9, -55, -30)$	Rt. DCDN $0 \leq s \leq 10$ SUIT $(x, y, z) = (11, -56, -30)$	Rt. VRDN $20 \leq s \leq 30$ SUIT $(x, y, z) = (4, -46, -25)$	Rt. VCDN $45 \leq s \leq 55$ SUIT $(x, y, z) = (-1, -29, -5)$
		r, p value			
Communication	HFA + LFA	−0.02, 0.928	0.10, 0.647	**0.60, 0.002***	**0.57, 0.005***
	HFA	−0.33, 0.321	−0.19, 0.567	0.62, 0.043	0.54, 0.049
	LFA	0.13, 0.692	0.02, 0.940	0.06, 0.848	0.38, 0.218
Daily living skills	HFA + LFA	0.48, 0.021	0.49, 0.018	0.44, 0.034	0.29, 0.187
	HFA	0.41, 0.216	0.42, 0.202	−0.07, 0.846	0.03, 0.938
	LFA	**0.76, 0.004***	0.55, 0.050	0.40, 0.196	−0.03, 0.930
Socialization	HFA + LFA	0.07, 0.764	0.23, 0.291	0.36, 0.094	0.44, 0.038
	HFA	−0.08, 0.820	0.19, 0.579	−0.06, 0.866	0.34, 0.304
	LFA	0.02, 0.945	−0.16, 0.611	0.19, 0.564	0.12, 0.719
Motor skills	HFA + LFA	0.34, 0.145	0.39, 0.089	−0.02, 0.934	0.13, 0.598
	HFA	0.52, 0.049	0.42, 0.159	−0.19, 0.623	−0.25, 0.524
	LFA	−0.04, 0.918	0.13, 0.714	−0.43, 0.185	−0.02, 0.950
ABC	HFA + LFA	0.26, 0.234	0.35, 0.106	0.46, 0.027	0.45, 0.030
	HFA	0.17, 0.620	0.25, 0.454	0.14, 0.676	0.28, 0.407
	LFA	0.56, 0.049	0.40, 0.200	0.06, 0.847	0.16, 0.625

P value is the probability of getting a correlation as large as the observed value by random chance (95% confidence interval), when the true correlation is 0. The *r* and *p* values are given in bold face whenever the corresponding *p* value<0.01

ABC Autism Behavior Checklist, *Rt.* right, *DRDN* dorso-rostral dentate nuclei; *DCDN* dorso-caudal dentate nuclei, *VRDN* ventro-rostral dentate nuclei, *VCDN* ventro-caudal dentate nuclei, *r* Pearson product–moment correlation coefficient

*p value<0.01

inter-axonal volume. The overall effect is to decrease the diffusion barriers to axons that can result in increased RD and decreased FA. Thus, the profile of abnormalities (higher RD and lower FA) might reflect the microstructural abnormalities of thinner and more numerous axons at dentatorubrothalamic pathways of ASD. Changes in both axon size and myelination have been reported in study of postmortem ASD brain. There was a decrease in the number of largest axons and an excessive number of thin axons in anterior cingulate, whereas axons in orbital frontal cortex showed decreased myelin thickness [53]. These changes in axon size and myelin thickness were associated with increased expression of the GAP-43, which the investigators hypothesize is related to changes in axon growth and myelination. Furthermore, changes in GAP-43 expression may induced by growth factors related to brain inflammation reported in ASD postmortem studies [54]. Our finding of changes in focal segments of the tracts is intriguing and may be related to inflammatory processes, as well as reports of presence of anti-myelin antibodies in sera of children with autism [55] and their mothers [56].

Technical Limitations

In this study, we employed the QBI technique to isolate multiple crossing fibers in clinical DTI data that were acquired at relatively smaller number of gradient directions and in lower *b* value than those of conventional HARDI data. The choice of spherical sampling radius in q-space (i.e., *b* value) depends on the desired angular resolution, available signal-to-noise ratio, and gradient performance specifications. In practice, *b* values of 3,000 s/mm^2 or greater are typically required in order to distinguish among different intra-voxel fiber populations [57]. Although we demonstrated that the QBI reconstruction technique with Laplace–Beltrami regularization [50] can reliably estimate the ODF in HARDI data acquired at a *b* value of 1,000, lower *b* value for the QBI reconstruction is suboptimal to resolve multiple fibers at higher angular resolution and might result in increasing false-negative tractography. Nonetheless, it provides a direct way to isolate complex neuronal pathways from clinical DTI acquisition.

Dentatorubrothalamocortical Pathway in Autism

Projections of dorsal dentate nucleus are related to motor function, whereas ventral/caudal projections are related to language and cognitive functions of the cerebellum [58]. Decreased white matter integrity in both dorsal and ventral portions of the tract may be related to motor, language, and cognitive features in autism. These findings are consistent with our previous PET study showing altered tryptophan metabolism in the dentatothalamocortical pathway in autism

Table 4 Correlation between behavioral domains and RD values of TBM segments

Domain	Group	r, p value			
		Rt. DRDN $0 \leq s \leq 10$ SUIT $(x, y, z) = (9, -55, -30)$	Rt. DCDN $0 \leq s \leq 10$ SUIT $(x, y, z) = (11, -56, -30)$	Rt. VRDN $20 \leq s \leq 30$ SUIT $(x, y, z) = (4, -46, -25)$	Rt. VCDN $45 \leq s \leq 55$ SUIT $(x, y, z) = (-1, -29, -5)$
Communication	HFA + LFA	0.37, 0.084	0.02, 0.929	−0.39, 0.060	−0.40, 0.053
	HFA	**0.62, 0.042**	0.10, 0.774	**−0.65, 0.030**	−0.60, 0.051
	LFA	0.30, 0.346	0.24, 0.447	−0.33, 0.271	−0.35, 0.241
Daily living skills	HFA + LFA	−0.39, 0.059	−0.37, 0.085	−0.33, 0.127	−0.11, 0.626
	HFA	−0.42, 0.198	−0.55, 0.081	0.20, 0.560	0.14, 0.685
	LFA	**−0.57, 0.041**	−0.33, 0.297	−0.19, 0.560	−0.02, 0.951
Socialization	HFA + LFA	0.10, 0.638	−0.14, 0.537	−0.17, 0.430	−0.18, 0.423
	HFA	0.08, 0.809	−0.11, 0.738	0.45, 0.161	−0.24, 0.475
	LFA	0.05, 0.875	−0.10, 0.754	−0.02, 0.952	0.02, 0.953
Motor skills	HFA + LFA	−0.27, 0.250	−0.29, 0.211	−0.11, 0.657	0.10, 0.660
	HFA	−0.62, 0.072	−0.65, 0.058	0.13, 0.734	0.36, 0.337
	LFA	−0.13, 0.713	−0.10, 0.772	0.16, 0.646	0.16, 0.649
ABC	HFA + LFA	0.02, 0.922	−0.22, 0.314	−0.32, 0.138	−0.13, 0.548
	HFA	−0.07, 0.844	−0.34, 0.308	0.22, 0.509	−0.13, 0.707
	LFA	−0.12, 0.701	−0.22, 0.498	−0.06, 0.857	0.19, 0.544

P value is the probability of getting a correlation as large as the observed value by random chance (95% confidence interval), when the true correlation is 0. The r and p value are given in bold face whenever the corresponding p value < 0.05

ABC Autism Behavior Checklist, *Rt.* right, *r* Pearson product–moment correlation coefficient

[59]. Our previous PET study using α-[11C] methyl-L-tryptophan as a tracer for serotonin synthesis reported that autistic boys showed *decreased* serotonin synthesis in the left frontal cortex and thalamus and *increased* serotonin synthesis in the right dentate nucleus [59]. The finding of the present study suggesting reduced integrity of the right dentatorubrothalamocortical pathway may be related to the serotonergic abnormalities in the nuclei connected by this pathway.

Cerebellum in Autism

Alteration in the cerebellar circuitry has been considered a neuropathological feature of ASD. Several studies have reported significant reductions in Purkinje cells in autistic brain [5, 9, 60, 61]. Using situ hybridization histochemistry, Yip et al. [8] showed three major subpopulations of dentate neurons in human brain: (1) the larger sized GABAergic dentate cells that project exclusively to the inferior olivary complex, (2) the smaller GABAergic dentate neurons that project to other dentate neurons, and (3) unlabeled neurons that project to thalamus, red nucleus, and/or brain stem nuclei. A significant reduction in GAD65 mRNA levels in the larger cell population but not in the small-sized cell population was observed; this reduction may disrupt the firing synchrony of inferior olivary neurons and the timing of Purkinje cell firing in the cerebellar circuitry. The simplest and most straightforward interpretation regarding an alteration in cerebellar circuitry in ASD is that a decreased volume of viable tissue due to a reduction in Purkinje cells will lead to abnormally reduced structural morphometry and functional activation. Many structural MRI studies have shown that people with ASD show significant morphological variations in the cerebellum [10, 11, 13]. However, controversy remains concerning the nature and the consistency of cerebellar alterations in gray matter and white matter of ASD. For instance, Courchesne et al. [62] showed relatively increased white matter in ASD (from 2 to 3 years old), less gray matter in ASD (at all ages), and reduced volumes of lobules VI–VII in ASD (at all ages). McAlonan et al. [63] reported that white matter volume in cerebellum is reduced in ASD but not statistically significant. Also, Palmen et al. [60] reported that high functioning children with ASD show a global increase in gray matter, but not white matter and cerebellar volume, proportional to the increase in brain volume. Recent work by Scott et al. [15] and Hodeg et al. [17] demonstrated no significant differences in the volume of white matter in cerebellum between controls and children with ASD. These findings correspond to the results of our study showing no significant changes in volumes of bilateral dentatorubrothalamocortical pathways in ASDs.

fMRI investigations using saccadic and pursuit eye movement paradigms [14] showed that children with HFA had

greater bilateral activation in a frontostriatal circuit including dorsolateral prefrontal cortex, caudate nucleus, medial thalamus, anterior and posterior cingulate cortex, and right dentate nucleus, indicating that systems dedicated to cognitive function (prefrontal–striatal–thalamocortical circuitry) may need to compensate for a disturbance in lower level sensorimotor systems. Another fMRI study using an appositional finger tapping paradigm [16] reported that the HFA group showed reduced activation in the ipsilateral anterior cerebellum, indicating diffusely decreased connectivity across the motor activation network relative to control children. Decreased cerebellar activation in the HFA group may reflect difficulty shifting motor execution from cortical regions associated with effortful control to regions associated with habitual execution. The dissociation of cerebral and cerebellar motor network in the ASD group might be related to our finding, involving a significant decrease in FA of right dorso-rostral dentatothalamocortical pathway of the ASD groups. This pathway is one component of the dentatothalamocortical pathways associated with motor function in dentate nucleus [18, 19]. Similarly, reduced FA in the right dorso-caudal and ventro-caudal dentatothalamocortical pathway of the LFA group may indicate an abnormality of caudal dentate nucleus in the LFA group that is mainly involved with non-motor functional deficits such as cognition/language function [18, 19]. This interpretation is bolstered by the finding within the children with ASD that FA for the ventral–rostral segment of the dentate nucleus was associated with communication skills, whereas the dorsal–rostral segment was more associated with motor functions. In conclusion, taken together with the findings of previous structural and functional MRI studies, our results demonstrate that abnormalities in the axonal integrity of cerebellar white matter may contribute to the behavioral phenotype in ASD.

References

1. Bauman ML, Kemper TL. Histoanatomic observations of the brain in early infantile autism. Neurology. 1985;35(6):866–74.
2. Ritvo ER, Freeman BJ, Scheibel AB, Duong T, Robinson H, Guthrie D, et al. Lower Purkinje cell counts in the cerebella of four autistic subjects: initial findings of the UCLA-NSAC autopsy research report. Am J Psychiatry. 1986;143(7):862–6.
3. Bailey A, Luthert P, Dean A, Harding B, Janota I, Montgomery M, et al. A clinicopathological study of autism. Brain. 1998;121(Pt 5):889–905.
4. Bauman ML, Kemper TL. Neuroanatomic observations of the brain in autism: a review and future directions. Int J Dev Neurosci. 2005;23(2–3):183–7.
5. Whitney ER, Kemper TL, Rosens DL, Bauman ML, Blatt GJ. Density of cerebellar basket and stellate cells in autism: evidence for a late developmental loss of Purkinje cells. J Neurosci Res. 2009;87(10):2245–54.
6. Fatemi SH, Halt AR, Realmuto G, Earle J, Kist DA, Thuras P, et al. Purkinje cell size is reduced in cerebellum of patients with autism. Cell Mol Neurobiol. 2002;22(2):171–5.
7. Batini C, Compoint C, Buisseret-Delmas H, Danile M, Guegan M. Cerebellar nuclei and the nucleocrotical projections in the rat: retrograde tracking coupled to GABA and glutatame immunohistochemistry. J Comp Neurol. 1992;315(1):74–84.
8. Yip J, Soghomonian JJ, Blatt GJ. Decreased GAD65 mRNA levels in select subpopulations in the cerebellar dentate nuclei in autism: an in situ hybridization study. Autism Res. 2009;2(1):50–9.
9. Yip J, Soghomonian JJ, Blatt GJ. Decreased GAD67 mRNA levels in cerebellar Punkinje cells in autism: pathophysiological implications. Acta Neuropathol. 2007;113(5):559–68.
10. Abell F, Krams M, Ashburner J, Passingham R, Friston K, Frackowiak R, et al. The neuroanatomy of autism: a voxel-based whole brain analysis of structural scans. Neuroreport. 1999;10(8):1647–51.
11. McAlonan GM, Daly E, Kumari V, Critchley HD, van Amlsvoort T, Suckling J, et al. Brain anatomy and sensorimotor gating in Asperger's syndrome. Brain. 2002;125(Pt 7):1584–606.
12. Allen G, Courchesne E. Differential effects of developmental cerebellar abnormality on cognition and motor functions in the cerebellum: an fMRI study of autism. Am J Psychiatry. 2003;160(2):262–73.
13. Akshoomoff N, Lord C, Lincoln AJ, Courchesne RY, Carper RA, Townsend J, et al. Outcome classification of preschool children with autism spectrum disorders using MRI brain measures. J Am Acad Child Adolesc Psychiatry. 2004;43(3):349–57.
14. Takarae Y, Minshew NJ, Luna B, Sweeney JA. Atypical involvement of frontostriatal systems during sensorimotor control in autism. Psychiatry Res. 2007;156(2):117–27.
15. Scott JA, Schumann CM, Goodlin-Jones BL, Amaral DG. A comprehensive volumetric analysis of the cerebellum in children and adolescents with autism spectrum disorder. Autism Res. 2009;2(5):246–57.
16. Mostofsky SH, Powel SK, Simmonds DJ, Goldberg MC, Caffo B, Pekar JJ. Decreased connectivity and cerebellar activity in autism during motor task performance. Brain. 2009;132(Pt 9):2413–25.
17. Hodge SM, Makris S, Kennedy DN, Caviness Jr VS, Howard J, McGrath L, et al. Cerebellum, language, and cognition in autism and specific language impairment. J Autism Dev Disord. 2010;40(3):300–16.
18. Dum RP, Strick PL. An unfolded map of the cerebellar dentate nucleus and its projections to the cerebral cortex. J Neurophysiol. 2003;89(1):634–9.
19. Küper M, Dimitrova A, Thürling M, Maderwald S, Roths J, Elles HG, et al. Evidence for a motor and a non-motor domain in the human dentate nucleus—an fMRI study. Neuroimage. 2011;54(4):2612–22.
20. Barnea-Goraly N, Kwon H, Menon V, Eliez S, Lotspeich L, Reiss AL. White matter structure in autism: preliminary evidence from diffusion tensor imaging. Biol Psychiatry. 2004;55(3):323–6.
21. Ben Bashat D, Kronfeld-Duenias V, Zachor DA, Ekstein PM, Hendler T, Tarrasch R, et al. Accelerated maturation of white matter in young children with autism: a high b value DWI study. Neuroimage. 2007;37(1):40–7.
22. Keller TA, Kana RK, Just MA. A developmental study of the structural integrity of white matter in autism. Neuroreport. 2007;18(1):23–7.
23. Lee JE, Bigler ED, Alexander AL, Lazar M, BuBray MB, Chung MK, et al. Diffusion tensor imaging of white matter in the superior temporal gyrus and temporal stem in autism. Neurosci Lett. 2007;424(2):127–32.

24. Sundaram SK, Kumar A, Makki MI, Behen ME, Chugani HT, Chugani DC. Diffusion tensor imaging of frontal lobe in autism spectrum disorder. Cereb Cortex. 2008;18(11):2659–65.

25. Kumar A, Sundaram SK, Sivaswamy L, Behen ME, Makki MI, Ager J, et al. Alterations in frontal lobe tracts and corpus callosum in young children with autism spectrum disorder. Cereb Cortex. 2010;20(9):2103–13.

26. Cheng Y, Chou KH, Chen IY, Fan YT, Decety J, Lin CP. Atypical development of white matter microstructure in adolescents with autism spectrum disorders. Neuroimage. 2010;50(3):873–82.

27. Mori S, Crain BJ, Chacko VP, van Zijl PC. Three-dimensional tracking of axonal projections in the brain by magnetic resonance imaging. Ann Neurol. 1999;45(2):265–9.

28. Basser PJ, Pajevic S, Pierpaoli C, Duda J, Aldroubi A. In vivo fiber tractography using DT-MRI data. Magn Reson Med. 2000;44 (4):625–32.

29. Koch MA, Glauche V, Finsterbusch J, Nolte UG, Frahm J, Weiller C, et al. Distortion-free diffusion tensor imaging of cranial nerves and of inferior temporal and orbitofrontal white matter. Neuroimage. 2002;17(1):497–506.

30. Tuch DS. Q-ball imaging. Magn Reson Med. 2004;52(6):1358–71.

31. Tuch DS, Resse TG, Wiegell MR, Wedeen VJ. Diffusion MRI of complex neural architecture. Neuron. 2003;40(5):885–95.

32. Hess CP, Mukherjee P, Han ET, Xu D, Vigneron DB. Q-ball reconstruction of multimodal fiber orientations using the spherical harmonic basis. Magn Reson Med. 2006;56(1):104–17.

33. Descoteaux M, Angelino E, Fitzgibbons S, Deriche R. Apparent diffusion coefficients from high angular resolution diffusion imaging: estimation and applications. Magn Reson Med. 2006;56 (2):395–410.

34. Kuo L, Chen J, Wedeen VJ, Tseng WI. Optimization of diffusion spectrum imaging and q-ball imaging on clinical MRI system. Neuroimage. 2008;41(11):7–18.

35. Deriche R, Calder J, Descoteaux M. Optimal real-time Q-ball imaging using regularized Kalman filtering with incremental orientation sets. Med Image Anal. 2009;13(4):564–79.

36. Diedrichsen J. A spatially unbiased atlas template of the human cerebellum. Neuroimage. 2006;33(1):127–38.

37. Diedrichsen J, Maderwald S, Küper M, Thürling M, Rabe K, Gizweski ER, et al. Imaging the deep cerebellar nuclei: a probabilistic atlas and normalization procedure. Neuroimage. 2010;54 (3):1786–94.

38. O'Donnell LJ, Westin CF, Golby AJ. Tract-based morphometry for white matter group analysis. Neuroimage. 2009;45(3):832–44.

39. Jeong JW, Kumar A, Sundaram SK, Chugani HT, Chugani DC. Aberrant diffusion and geometric properties in the left arcuate fasciculus of developmentally delayed children: a diffusion tensor imaging study. Am J Neuroradiol. 2011;32(2):323–30.

40. Smith SM, Jenkinson M, Johansen-Berg H, Rueckert D, Nichols TE, Mackay CE, et al. Tract-based spatial statistics: voxelwise analysis of multi-subject diffusion data. Neuroimage. 2006;31 (4):1487–505.

41. Lord C, Rutter M, Le Couteur A. Autism diagnostic interview-revised: a revised version of a diagnostic interview for caregivers of individuals with possible pervasive developmental disorders. J Autism Dev Disord. 1994;24(5):659–85.

42. Constantino JN, Przybeck T, Friesen D, Todd RD. Reciprocal social behavior in children with and without pervasive developmental disorders. J Dev Behav Pediatr. 2000;21(1):2–11.

43. Constantino JN, Davis SA, Todd RD, Schindler MK, Gross MM, Brophy SL, et al. Validation of a brief quantitative measure of

44. autistic traits: comparison of the social responsiveness scale with the autism diagnostic interview-revised. J Autism Dev Disord. 2003;33(4):427–33.

44. Wechsler D. Wechsler preschool and primary scale of intelligence, 3rd edition (WPPSI-III). San Antonio: The Psychological Corporation; 2002.

45. Wechsler D. Wechsler intelligence scale for children—fourth edition: administrative and scoring manual. San Antonio: The Psychological Corporation; 2003.

46. Sattler JM, Dumont R. Assessment of children: WISC-IV and WISC-III supplement. San Diego, CA: Author; 2004.

47. Mullen EM, editor. Mullen scales of early learning. Circle Pines: American Guidance Service Inc.; 1995.

48. Sparrow SS, Balla DA, Cicchetti DV, Doll EA. Vineland adaptive behavior scales. Circle Pines: American Guidance Service; 1984.

49. Perry A, Factor DC. Psychometric validity and clinical usefulness of the Vineland Adaptive Behavior Scales and the AAMD Adaptive Behavior Scale for an autistic sample. J Autism Dev Disord. 1989;19(1):41–55.

50. Descoteaux M, Angelino E, Fitzgibbons S, Deriche R. Regularized, fast, and robust analytical Q-ball imaging. Magn Reson Med. 2007;58(3):497–510.

51. Wedeen VJ, Wang RP, Schmahmann JD, Benner T, Tseng WY, Dai G, et al. Diffusion spectrum magnetic resonance imaging (DSI) tractography of crossing fibers. Neuroimage. 2008;41(4):1267–77.

52. Holm S. A simple sequentially rejective multiple test procedure. Scand J Stat. 1979;6(2):65–70.

53. Zikopoulos B, Barbas H. Changes in prefrontal axons may disrupt the network in autism. J Neurosci. 2010;30(44):14595–609.

54. Vargas DL, Nascimbene C, Krishnan C, Zimmerman AW, Pardo CA. Neuroglial activation and neuroinflammation in the brain of patients with autism. Ann Neurol. 2005;57(1):67–81.

55. Singh VK, Warren RP, Odell JD, Warren WL, Cole P. Antibodies to myelin basic protein in children with autistic behavior. Brain Behav Immun. 1993;7(1):97–103.

56. Singer HS, Morris CM, Gause CD, Gillin PK, Crawford S, Zimmerman AW. Antibodies against fetal brain in sera of mothers with autistic children. J Neuroimmunol. 2008;194(1–2):165–72. Epub 2008 Feb 21.

57. Frank LR. Anisotropy in high angular resolution diffusion-weighted MRI. Magn Reson Med. 2001;45(6):935–9.

58. Strick PL, Dum RP, Fiez JA. Cerebellum and nonmotor function. Annu Rev Neurosci. 2009;32:413–34.

59. Chugani D, Muzik O, Rothermel R, Behen M, Chakraborty P, Mangner T, et al. Altered serotonin synthesis in the dentato-thalamocortical pathway in autistic boys. Ann Neurol. 1997;42 (4):666–9.

60. Palmen SJ, van Engeland H, Hof PR, Schmitz C. Neuropathological findings in autism. Brain. 2004;127(Pt 12):2572–83.

61. Guptill JT, Booker AB, Gibbs TT, Kemper TL, Bauman ML, Blatt GJ. [3H]-flunitrazepam-labeled benzodiazepine binding sites in the hippocampal formation in autism: a multiple concentration autoradiographic study. J Autism Dev Disord. 2007;37(5):911–20.

62. Courchesne E, Karns CM, Davis HR, Ziccardi R, Carper RA, Tigue ZD, et al. Unusual brain growth patterns in early life in patients with autistic disorder: an MRI study. Neurology. 2001;57 (2):245–54.

63. McAlonan GM, Cheung V, Cheung C, Suckling J, Lam GY, Tai KS, et al. Mapping the brain in autism. A voxel-based MRI study of volumetric difference and intercorrelations in autism. Brain. 2005;128(Pt2):268–76.